On the Suitability of Light Field Imaging for Road Surface Crack Detection

David Fernandes, Paulo Lobato Correia
Instituto Superior Técnico, Universidade de Lisboa / Instituto de Telecomunicações

Henrique Oliveira
Instituto Politécnico de Beja / Instituto de Telecomunicações

Abstract

During traditional road surveys, inspectors capture images of pavement surface using cameras that produce 2D images, which can then be automatically processed to get a road surface condition assessment. In this paper the use of a light field imaging sensor is proposed, notably the Lytro Illum camera, to explore whether the richer information captured by this imaging sensor provides additional cues useful to improve the automatic detection of road surface cracks. The preliminary results obtained indicate the interest in further exploring the disparity information captured by the light field sensor.

1 Introduction

This paper explores the potential of using of a light field camera, the Lytro Illum, to improve the automatic detection of road surface cracks, when compared to the usage of conventional 2D cameras.

Light field cameras are emerging as powerful sensor devices that capture the full spatio-angular visual information in a viewing range. This means that the light field information can be processed to obtain a matrix of 2D images, the sub-aperture images, corresponding to slightly different perspectives of the scene. This allows exploring the disparity between the various sub-aperture images, potentially making road cracks more salient and easier to detect.

The matrix of sub-aperture images can be computed from the raw light field with the help of the Matlab Light Field Toolbox [1].

To evaluate the potential of light field imaging for crack detection, a small dataset was captured in conditions similar to those considered during traditional road pavement surveys, with the camera positioned at 1 *m* from the pavement surface, with its optical axis perpendicular to the road pavement.

This paper considers two simple crack detection systems: (i) a simple 2D crack detection system, *2D_Crack_Detector*, which is used for comparison purposes; and (ii) the proposed light field crack detector *LF_Crack_Detector*, which uses the matrix of sub-aperture images computed form the light field information. Both systems use the same image processing techniques to obtain the final crack detection results, without focusing on optimizing the performance of the systems, but rather focusing on the initial detection stage, to evaluate the potential of exploring the light field disparity information for improving the detection of cracks.

2 Crack Detection

This section details the main modules composing each of the crack detection systems considered. Section 2.1 details the conventional 2D crack detector pipeline, whose architecture is shown in Figure 1 (a), while Section 2.2 details the proposed light field system – see Figure 1 (b).

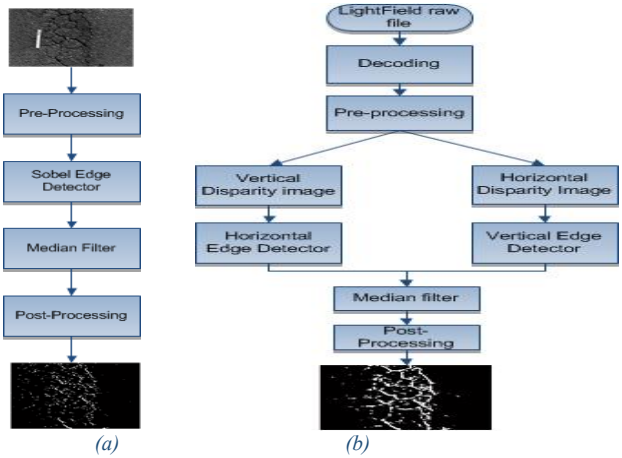

Figure 1: System architecture (a) 2D_Crack_Detector, (b) LF_Crack_Detector

2.1 2D Crack Detector

The considered 2D system follows the architecture of Figure 1(a). A simple set of techniques were considered for illustration purposes, which can later be improved, for instance considering those presented in [2][3] . The system takes as input a grayscale image, and then follows the steps briefly explained here, and whose results are illustrated in Figure 2: **(1) Saturation,** since it is assumed that crack pixels are darker than non-crack pixels, those pixels with high intensities can replaced with an intensity value that is clearly above the crack intensities, but allowing to reduce the intensity variance. **(2) Sobel edge detector**, a Sobel mask is applied to detect the edges in the image, although it often also amplifies the existing noise. **(3) Median Filter**, with a window size of 5x5 pixels, is used to remove some of the image noise. **(4) Post-Processing**, considers a Gaussian Blur filter, with a standard deviation value of 2, to further reduce noise and to soften the detected crack edges. Finally, a thresholding operation is applied to generate the image where candidate crack pixels are identified. The threshold value used is 25, all the pixels with intensity value above 25 are identified as belonging to a crack.

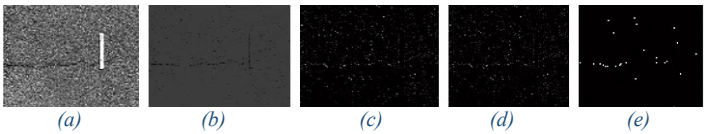

Figure 2: Results of each processing step of the 2D system: (a) Original Image, (b) Step 1, (c) Step 2, (d) Step 3, (e) Step 4. (Images are shown with increased brightness for easier visualization)

2.2 Proposed Light Field Crack Detector

Since the raw light field (LF) includes more information than a simple 2D image, the proposed LF crack detector exploits the captured disparity for improving the detection of cracks.

The **Decoding** step, takes the raw light field and creates a 15x15 matrix of 2D sub-aperture images, each with spatial resolution 435x625 pixels and representing a slightly different perspective – see Figure 3 (a).

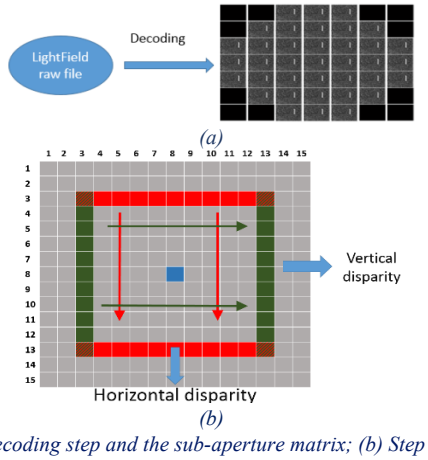

Figure 3: (a) Decoding step and the sub-aperture matrix; (b) Step (3) - Vertical and Horizontal disparity computation illustration.

The **Pre-processing** step has same purpose as the saturation step in section 2.1, i.e., to remove some of the image noise.

To exploit the disparity present in the light field images, a selection of sub-aperture images is considered after some experimentation, and also according to [4] considering the difference between images at position symmetrical to the central sub-aperture image. Figure 3 (b) illustrates the **Vertical (resp. Horizontal) Disparity Image** creation, when subtracting the images of column (resp. row) 3 with those of column (resp. row) 13 of the matrix, and summing the obtained differences.

Figure 4 shows the summation results when considering different amounts of disparity, i.e. columns (resp. rows) closer or further apart from each other. The number of the used sub-aperture images considered in each column (resp. row) can also be varied, as illustrated in Figure 6.

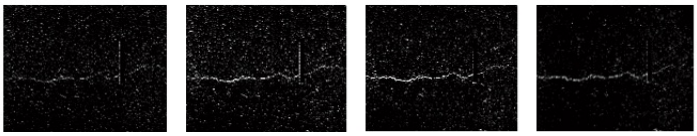

(a) (b) (c) (d)

Figure 4: (a) 7ª and 9ª rows and columns, (b) 5ª and 11ª row and columns (c) 3ª and 13ª rows and columns (d) 1ª and 15ª rows and columns

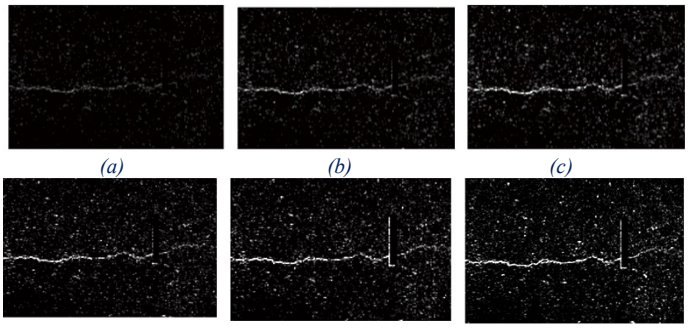

(a) (b) (c) (c) (d) (e)

Figure 6: Number of Images used (a) 1 images, (b) 3 images, (c) 5 images, (d) 7 images, (e) 9 images, (f) 11 images.

Summation of the horizontal and vertical disparities is illustrated in Figure 7 (left and right), capturing the crack information present in the specified direction.

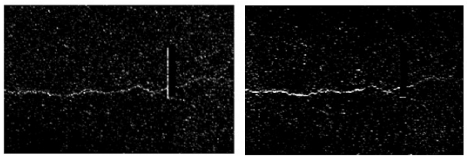

Figure 7: Sum of the horizontal differences (left), sum of the vertical differences (right).

Eventually, an **edge detector** can be applied to the horizontal and vertical disparity images to use the same processing pipeline as applied to the 2D images, thus enhancing the crack details. The sum of both images - see Figure 8 (right) is the best capturing all the crack information present in the image.

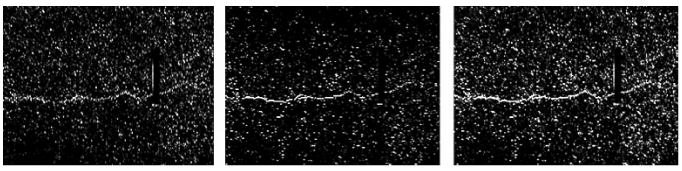

Figure 8: Step 3: Vertical mask (left), Horizontal mask (centre), Sum of the previous images (right).

The **edge detector** enhances the crack details but it also increases the noise present in the non-crack areas.
To reduce the effect of noise, the same non-linear filtering technique, **2-D median filter**, with a window size of 5x5 pixels, can be applied, as illustrated in Figure 9.

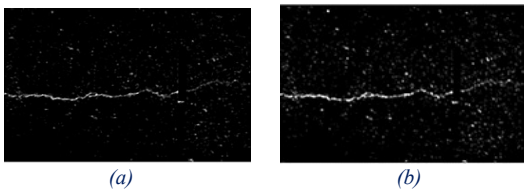

(a) (b)

Figure 9: Median filter applied: (a) without the Sobel step; (b) after the Sobel detector.

The final step, **Post-Processing**, performs a thresholding operation with a chosen threshold value of 64, to identify the crack pixels, after applying a Gaussian filter, with a standard deviation value of 2, to smooth the noise in the non-crack areas. The results are illustrated in Figure 10.

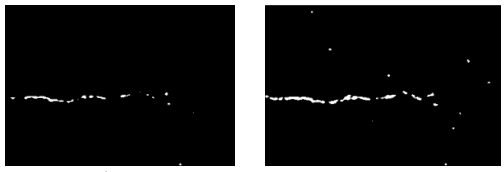

(a) (b)

Figure 10: Results of the post-processing step (a) without and (b) with the application of the Sobel detector.

These results show that a transversal crack can be easily identified in Figure 10. The threshold values and other parameters used are the same during the processing of both the images. The difference between them is due to the usage of an edge detector, adopted to enhance the edges, although the presence of groups of pixels presenting small dimension in the image may occur.

3 Discussion and Conclusions

Figure 11 includes a set of additional results considering both the 2D and the proposed light field crack detection systems.

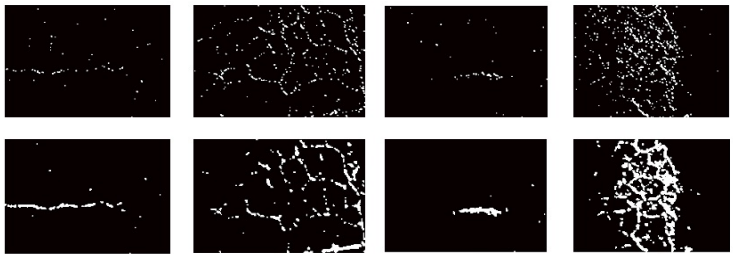

(a) (b) (c) (d)

Figure 11: Results of both systems on 4 images (first row: 2D crack detector; second row: light field crack detector): (a) Image 1, (b) Image 2, (c) Image 3, (d) Image 4

As a conclusion, the usage of light field imaging, with some basic image processing techniques, seems to provide better crack detection results, than using the same techniques over a 2D image (in this case the central 2D sub-aperture image). Exploring the light field disparity information showed a better definition of the cracks present in the test images.
Future work involves considering a more sophisticated and complex image processing and classification techniques in the proposed system architecture. Also, the acquisition of a larger test image dataset and an elaboration of a quantitative measure like the F-measure metric will be addressed in a further work.

References

[1] D. G. Dansereau, "Light Field Toolbox for Matlab," vol. 34, no. 2, pp. 2013–2015, 2013.

[2] H. Oliveira and P. L. Correia, "Automatic road crack detection and characterization," *IEEE Trans. Intell. Transp. Syst.*, vol. 14, no. 1, pp. 155–168, 2013.

[3] R. Amhaz, S. Chambon, J. Idier, and V. Baltazart, "Automatic Crack Detection on Two-Dimensional Pavement Images: An Algorithm Based on Minimal Path Selection," *IEEE Trans. Intell. Transp. Syst.*, vol. 17, no. 10, pp. 2718–2729, 2016.

[4] A. Sepas-Moghaddam, P. Correia and F. Pereira, "Light field local binary patterns description for face recognition," in *IEEE ICIP*, Beijing, China, Sep. 2017

Acknowledgement

This work has been partially supported by Instituto de Telecomunicações under Fundação para a Ciência e Tecnologia, Grant UID/EEA/ 50008/2013.